Research Article

Received: 28 June 2020 Revised: 5 August 2020 Accepted article published: 25 August 2020 Published online in Wiley Online Library: 10 September 2020

(wileyonlinelibrary.com) DOI 10.1002/pi.6103

Understanding the effects of montmorillonite and sepiolite on the properties of solution-cast chitosan and chitosan/silk peptide composite films

Pei Chen,[a] Fengwei Xie[b,c†*] and Tony McNally[b*]

Abstract

Blending with another biopolymer or nanomaterial can be an effective route to modify or tailor the properties of chitosan materials. In this work, we compared the effects of two nanoclays, montmorillonite (MMT) and sepiolite (SPT), on the properties of chitosan and chitosan/silk peptide (SP) films. While the solution-cast chitosan/SP films showed no phase separation on a micron length scale, some degree of molecular-level heterogeneity or incompatibility was evident. MMT nanoplatelets were delaminated in the chitosan-alone matrix, resulting in enhanced mechanical properties and hydrophobicity. In comparison, inclusion of SPT nanoneedles was less effective at altering the properties of the chitosan matrix. In the chitosan/SP system, the MMT was poorly dispersed, suggesting the two biopolymers interfere with how each interacts with the nanoclay. Nonetheless, in this case, MMT disrupted biopolymer chain interactions, leading to reduced mechanical properties and increased surface hydrophilicity. In contrast, SPT was found to enhance the mechanical properties of the chitosan/SP matrix, certainly associated with it being better dispersed. Thus, this work shows the efficacy of MMT and SPT as a route to altering the structure and properties of chitosan-based biopolymer matrices.

Supporting information may be found in the online version of this article.

Keywords: chitosan; silk peptide; nanoclay; nanocomposites; mechanical properties; surface hydrophilicity

INTRODUCTION

Natural biopolymers are a unique class of polymers which have attracted huge interest in materials development due to their appealing advantages such as renewability, wide availability, low/non-toxicity, biodegradability and biocompatibility. Chitin, poly(β-(1,4)-*N*-acetyl-D-glucosamine), is the second most abundant naturally existing polysaccharide next to cellulose and can be readily extracted from crab and shrimp shells.[1] Deacetylation of chitin yields chitosan, a linear polysaccharide consisting of (1,4)-linked 2-amino-deoxy-β-D-glucan.[1,2] While chitin is not readily processable due to its insolubility in water and classic organic solvents, chitosan is soluble in mild acids and thus has been studied more extensively. The unique pseudo-natural cationic character of chitosan, provided by its fraction of ion pairs (–COO^- ^+H_3N–), has been widely discussed.[1] Chitosan has been found to have useful properties and functionality, such as antimicrobial and antifungal efficacy,[3–7] controlled release ability,[8–12] adsorption of dyes and metals[13–16] and oleophobicity,[17,18] and therefore chitosan has huge potential for application in active packaging and in the biomedical, environmental and agricultural sectors.

It is common to blend different biopolymers (e.g. chitosan and proteins) to achieve further enhanced properties and combined functionality. Torres-Giner *et al.*[19] suggested that the enhanced antimicrobial activity of chitosan/zein blends could be related to the entrapped acid released by zein. Chitosan/silk fibroin (SF) blend films can be used as a wound dressing and artificial skin because of their good mechanical properties and good water

* *Correspondence to: F Xie or T McNally, International Institute for Nanocomposites Manufacturing (IINM), WMG, University of Warwick, Coventry, CV4 7AL, UK. E-mail: d.xie.2@warwick.ac.uk, fwhsieh@gmail.com (Xie); E-mail: t.mcnally@warwick.ac.uk (McNally)*

† *This author leads the research.*

a *College of Food Science, South China Agricultural University, Guangzhou, Guangdong, 510642, China*

b *International Institute for Nanocomposites Manufacturing (IINM), WMG, University of Warwick, Coventry, CV4 7AL, UK*

c *School of Chemical Engineering, University of Queensland, Brisbane, Queensland, 4072, Australia*

vapour and oxygen permeability.[20] For bone tissue engineering, both chitosan and SF are non-toxic and have good biocompatibility, but are poor biological scaffolds when used alone.[21] It was found that the addition of SF reduced the degradation of chitosan-containing scaffolds in lysozyme solution and the blended scaffolds had higher compressive strength and modulus than the individual components.[22] In composite chitosan/SF nanofibres, it was revealed that chitosan enhanced osteogenic differentiation and SF promoted proliferation in the nanofibres.[23]

Moreover, for enhanced properties and functionality, composites of chitosan reinforced with various nanofillers have been widely studied.[13,24,25] Typically, chitosan materials reinforced with montmorillonite (MMT) have been shown to have improved mechanical properties,[26–29] improved thermal stability[29] and reduced water sensitivity.[7,26–28,30] Celis *et al.*[31] demonstrated that composites of chitosan and MMT can be used as an excellent absorbent for the removal of anionic pesticides from soil and water under mildly acidic conditions. Moreover, research has shown that the antimicrobial activity of chitosan could be enhanced with the incorporation of MMT[7] or MMT-supported Ag nanoparticles.[27,28] The enhancement in material properties was ascribed to the high chemical affinity between chitosan and MMT and the large surface area of this layered silicate. In particular, chitosan with its amine group protonated is a polycation and can effectively interact with the negatively charged layers of natural MMT, functioning as an organomodifier.[32,33]

Compared with composites of chitosan and MMT, chitosan modified with sepiolite (SPT) has been studied to a much lesser extent. Both MMT and SPT are negatively charged in their natural forms due to isomorphic substitutions occurring between platelets in the case of MMT.[32,34–36] While MMT is in the form of two-dimensional nanoplatelets, SPT is in the form of one-dimensional nanoneedles. Darder *et al.*[33,37] have shown the high affinity of chitosan for SPT as with MMT. However, few studies have been reported to directly compare the reinforcement effect between MMT and SPT on chitosan materials and their blends.

In this study, we investigated how inclusion of a low-molecular-mass SF (rather called silk peptide (SP)) and nanoclays (MMT and SPT) can affect the structure and properties of solution-cast chitosan and chitosan/SP films. The lower molecular mass could allow SP to be dissolved and processed more easily than SF. While MMT has a greater surface area than SPT, we propose that their efficacy at altering structure and properties depends on biopolymer matrix type. Furthermore, we also emphasise that these polymer blends were solution-mixed as previous work[38] using thermomechanical mixing of the same systems resulted in different behaviour.

EXPERIMENTAL

Materials

Chitosan (poly(β-(1,4)-D-glucosamine)), derived from crab shells, with a viscosity of about 100 mPa s (1% solution in 1% acetic acid at 25 °C), a weight-average molecular mass of *ca* 150 000 g mol^{-1} and a degree of deacetylation of >90% was purchased from Shanghai Ryon Biological Technology Co. Ltd (Shanghai, China). SP powder, derived from *Bombyx mori*, with a weight-average molecular mass of 500–30 000 g mol^{-1}, was supplied by Huzhou Xintiansi Bio-tech Co. Ltd (Huzhou, China). MMT K 10 (surface area 220–270 m^2 g^{-1}) and SPT were acquired from Sigma-Aldrich Co. Ltd (Dorset, UK), formic acid (98% w/w AR) and sodium bromide (pure) from Scientific Laboratory Supplies Ltd (Nottingham, UK), and toluene (AR) from Fisher Scientific UK Ltd (Loughborough, UK). Deionised water was used throughout the study.

Sample preparation

Table 1 shows the formulations of the different samples prepared. For sample preparation, 15 g of chitosan or the 1:1 (w/w) mixture of chitosan and SP was added into 530 mL of 0.1 mol L^{-1} formic acid solution (pH 2.38) in a beaker, and the suspension was stirred at 60 °C for 2 h using a magnetic stirrer. As this pH is below the isoelectric point (pI) of SP (3.8–3.9),[39] SP should also be positively charged as chitosan. As a result, a stable chitosan/SP solution could be formed without ionic complexation or precipitation. Meanwhile, MMT or SPT at a loading of 1.5 wt% or 3.0 wt% based on the biopolymer matrix was dispersed in 25 mL of 0.1 mol L^{-1} formic acid solution in a small vial, which was sonicated using a tip-type sonicator Hielscher UP200S (Hielscher Ultrasonics GmbH, Teltow, Germany) at 200 W and 24 kHz for 10 min. After 2 h stirring of the biopolymer suspension, the nanoclay suspension was poured into the biopolymer suspension and the mixture was stirred for another minute before being poured into a plastic container with a flat bottom. The container was ventilated at room temperature (RT) until a dried film was obtained. The cast films were stored in desiccators at 57% relative humidity (achieved using saturated NaBr) for 3 weeks. In the desiccators, an open beaker containing toluene was placed to avoid the samples becoming mouldy. After conditioning, the sheets were cut into dumbbell-shaped specimens according to type V of ASTM

Table 1. Sample codes and compositions (represented as portions by weight)

Sample	Chitosan	SP	MMT	SPT
CS	100	–	–	–
CS/M1.5	100	–	1.5	–
CS/M3.0	100	–	3.0	–
CS/S1.5	100	–	–	1.5
CS/S3.0	100	–	–	3.0
CSSP	50	50	–	–
CSSP/M1.5	50	50	1.5	–
CSSP/M3.0	50	50	3.0	–
CSSP/S1.5	50	50	–	1.5
CSSP/S3.0	50	50	–	3.0

Polymer International published by John Wiley & Sons Ltd on behalf of Society of Industrial Chemistry.

Standard D638-14. The samples were always stored hermetically before characterisation.

Characterisation

SEM imaging was carried out using a Zeiss Sigma field-emission scanning electron microscope (Carl Zeiss AG, Oberkochen, Germany) with an InLens detector, an acceleration voltage of 6 kV (for films) and an aperture of 20 μm. Before imaging, the biopolymer films were cryo-fractured using liquid nitrogen and sputter-coated with gold/palladium.

XRD measurements were performed using a PANalytical Empyrean X-ray diffractometer (Malvern Panalytical Ltd, Malvern, UK) with a Co target (Kα = 1.790307 Å) and a PIXcel1D (RTMS type) detector at 40 kV and 40 mA. Data were recorded for an angular range (2θ) of 6°–40°, with a step size of 0.0263° and a total scan time of 46 min. Crystal lattice spacing (*d*-spacing) is calculated according to Bragg's law:

$$d = \frac{n\lambda}{2\sin\theta}$$

where θ is the angle of incidence, λ is the wavelength of the incident light and n is an integer.

Fourier transform infrared (FTIR) spectra were recorded using a Bruker Tensor 27 FTIR spectrometer (Bruker Corporation, Billerica, MA, USA) with an attenuated total reflectance (ATR) accessory. Each spectrum was obtained based on 32 scans over the range 4000–500 cm^{-1} at RT (about 22 °C) at a resolution of 4 cm^{-1}. The background spectrum was recorded in air and subtracted from the sample spectrum.

Tensile testing was performed using an Instron 3367 universal testing machine (Norwood, MA, USA) with a 1 kN load cell at a constant crosshead speed of 3 mm min^{-1}. As the specimens were in the form of thin films, specimen extension was measured by grip separation as suggested in ASTM Standard D882. Young's modulus (E), tensile strength (σ_t) and elongation at break (ε_b) were automatically determined using Instron Bluehill 3 software from at least seven replicates for each sample.

Dynamic mechanical thermal analysis (DMTA) was carried out using a Tritec 2000 DMA instrument (Triton Technology Ltd, Nottinghamshire, UK) in tension mode and the length of the tension section tested was 10 mm. Temperature scans were carried out from −100 °C to 110 °C at a heating rate of 2 K min^{-1}, a frequency of 1 Hz and a displacement of 0.02 mm. The dynamic storage modulus (E'), loss modulus (E'') and loss tangent (tan $\delta = E''/E'$) were automatically calculated by the software.

TGA was performed using a Mettler Toledo TGA facility (Mettler Toledo, Columbus, OH, USA) from 25 to 700 °C at a heating rate of 10 K min^{-1} under nitrogen. For each measurement, a sample mass of *ca* 3 mg contained in a 70 μL alumina crucible was used.

Contact angle data were acquired from RT sessile tests based on the Young–Laplace equation using an Attension Theta Lite instrument (Biolin Scientific UK, Manchester, UK). As the contact angle kept changing after the water drop was placed on the biopolymer film surface, contact angles at 0 s and 60 s (θ_{c0s} and θ_{c60s}, respectively) were recorded.

RESULTS AND DISCUSSION

The SEM images (Fig. 1) show that, for all the formulations, films were successfully formed without apparent phase separation. CSSP/S1.5 showed some particle-like features on the surface (even protruding out from the surface), which could be due to agglomerated SPT nanoneedles and this feature was more dominant for CSSP/S3.0. CSSP/M3.0 also showed some particles on its surface, which in this instance could be agglomerated MMT, while no such feature was evident on CSSP/M1.5. In contrast, for the chitosan matrix, inclusion of either MMT or SPT did not cause

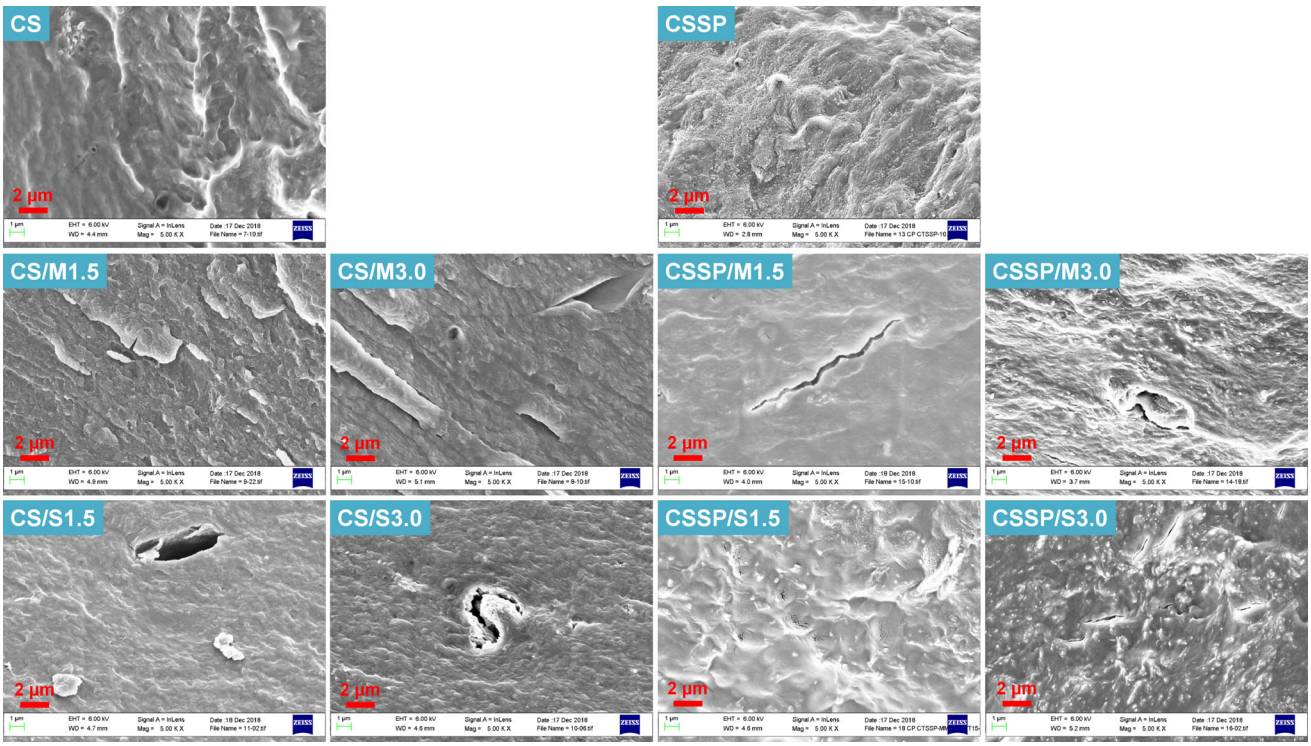

Figure 1. SEM images of cryo-fractured surfaces of the chitosan and chitosan/SP films with different MMT/SPT content (0 wt%, 1.5 wt% and 3.0 wt%).

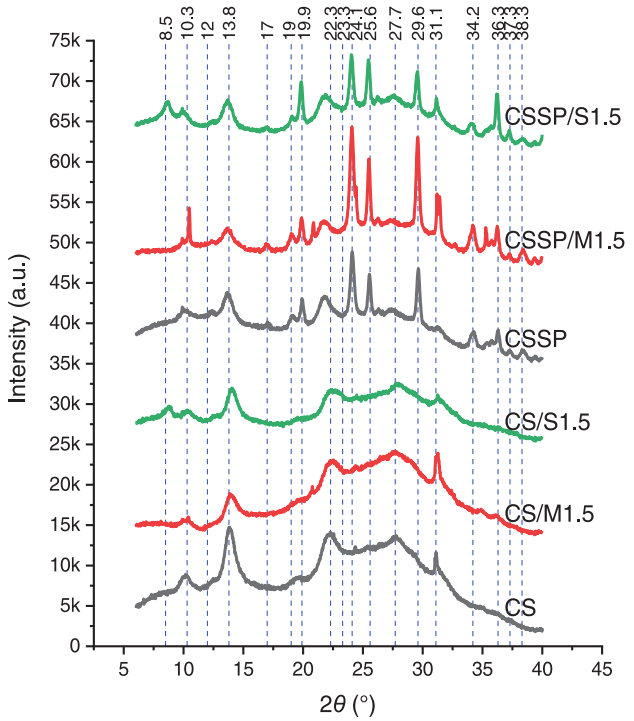

Figure 2. X-ray diffractograms for the chitosan and chitosan/SP films with different MMT/SPT content (0 wt%, 1.5 wt% and 3.0 wt%). The reference lines are characteristic peaks for MMT (10.3°), SPT (10.3°), chitosan (12°, 13.8° (new), 22.3° (shifted), 23.3°, 27.7° (new) and 31.1° (new)) and SP (17°, 19°, 19.9°, 24.1°, 25.6°, 29.6° (new), 34.2° (new), 36.3°, 37.3° and 38.3° (new)).

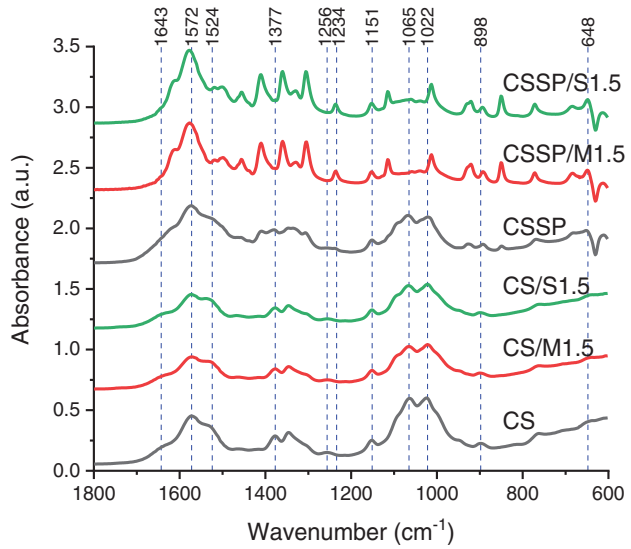

Figure 3. FTIR spectra for the chitosan and chitosan/SP films with different MMT/SPT content (0 wt%, 1.5 wt% and 3.0 wt%). The reference line indicates characteristic peaks of unprocessed chitosan (1643 cm^{-1}, 1572 cm^{-1}, 1377 cm^{-1}, 1256 cm^{-1}, 1151 cm^{-1}, 1065 cm^{-1}, 1022 cm^{-1} and 898 cm^{-1}) and unprocessed SP (1524 cm^{-1}, 1234 cm^{-1} and 648 cm^{-1}).

apparent changes to the surface morphology. The SEM observation here indicates that the MMT and SPT were more finely dispersed in the chitosan matrix than in the chitosan/SP matrix.

Figure 2 shows that the XRD curves for CS, CS/M1.5 and CS/S1.5 are similar to each other, with two major reflections at $2\theta \sim 22.3°$ ((100) reflection, *d*-spacing 0.46 nm) and 13.8° ((020) reflection, *d*-spacing 0.75 nm).[40] Besides, there were peaks at 10.2° (1.01 nm), 27.7° (0.37 nm) and 31.1° (0.33 nm). The X-ray diffractograms for these processed chitosan samples were quite different from that for unprocessed chitosan, with the latter having only two major peaks at $2\theta = 12.0°$ ((020) reflection, *d*-spacing 0.86 nm) and 23.3° ((100) reflection, *d*-spacing 0.44 nm).[38] Thus, the dissolution of chitosan completely destroyed the original crystalline structure and new crystals were formed in the solution-cast chitosan films. Compared with CS, CS/M1.5 and CS/S1.5 exhibited reduced peak intensities (especially at 10.2°, 13.8° and 22.3°), suggesting that the inclusion of nanoclays moderately suppressed chitosan recrystallisation.

CSSP displayed the characteristic peaks of processed chitosan at 10.2°, 13.8°, 22.3°, 27.7° and 31.1° 2θ. This blend film also showed reflections that are characteristic of SP but with shifts in peak position. These include the sharp peak at $2\theta = 24.1°$ (*d*-spacing 0.43 nm) and smaller peaks at $2\theta = 19.0°$ (0.54 nm), 25.6° (0.40 nm) and 36.3° (0.29 nm), which represent the silk I structure.[41,42] Besides, the peaks at $2\theta = 17.0°$ (*d*-spacing 0.61 nm), 19.9° (0.52 nm) and 37.3° (0.28 nm) are also derived from SP. Moreover, some new peaks at $2\theta = 29.6°$ (*d*-spacing 0.35 nm), 34.2° (0.30 nm) and 38.3 (0.27 nm) can be observed. Thus, CSSP exhibited a polymorph containing a silk I structure and other undefined structures. The silk II (antiparallel β-pleated sheet) structure[41–43] was not evident here. CSSP/M1.5 and CSSP/S1.5 displayed similar XRD diffractograms to that of CSSP suggesting that inclusion of MMT or SPT did not change the crystalline structures of the biopolymers.

Compared with their respective counterparts without MMT or SPT, both CS/S1.5 and CSSP/S1.5 exhibited an additional peak at 8.7° 2θ (*d*-spacing 1.18 nm), which could be ascribed to SPT (8.5° 2θ, *d*-spacing 1.21 nm)[38] as its zeolitic pores are not affected by processing whether in solution or 'melt' state. Compared with CSSP, CSSP/M1.5 displayed an additional sharp peak at 10.5° 2θ (*d*-spacing 0.98 nm), which is due to the interlayer spacing of MMT (10.3° 2θ, *d*-spacing 1 nm).[38] This suggests that MMT was not adequately delaminated in the chitosan/SP matrix. However, this sharp peak was not evident for CS/M1.5, and the MMT was more finely dispersed in the chitosan matrix than in the chitosan/SP matrix.

As shown in Fig. 3, CS, CS/M1.5 and CS/S1.5 displayed very similar FTIR spectra. Their FTIR patterns matched well to that of neat chitosan,[38] indicating that no chemical reactions occurred during processing, as expected. Also, inclusion of MMT or SPT did not cause any apparent changes to the FTIR spectra of the biopolymer matrices.

For CSSP, the characteristic bands of chitosan were evident, although some of these bands had shifted. There was a red shift for the bands at 1022 cm^{-1} (skeletal vibration (–C–O– stretching) of glucosamine) and a blue shift of the band at 1377 cm^{-1} (CH_3 symmetrical deformation mode).[44–46] The band at 1256 cm^{-1} (amide III)[44–46] almost disappeared. These shifts could reflect hydrogen-bonding interactions between chitosan and SP. The characteristic FTIR peaks of SP, just visible (e.g. 1408 cm^{-1}, 1327 cm^{-1}, 922 cm^{-1} and 851 cm^{-1}), were weak in CSSP. The intermolecular hydrogen-bonding interactions between the two biopolymers could be associated with the amide groups (containing –NH–) of SP and the carbonyl (C=O) and amino ($-NH_2$) groups of chitosan (not 100% deacetylated).[47–50] No absorption bands that are characteristic of the β-molecular conformation were seen here,[20,42,51–57] in agreement with the XRD data.

Polymer International published by John Wiley & Sons Ltd on behalf of Society of Industrial Chemistry.

CSSP/M1.5 and CSSP/S1.5 showed FTIR spectra quite different from that of CSSP, but containing strong characteristic bands from SP[38] (e.g. 1410 cm^{-1}, 1360 cm^{-1}, 1306 cm^{-1}, 1234 cm^{-1}, 1013 cm^{-1}, 920 cm^{-1} and 851 cm^{-1}).[42,51,55,56] The apparent blue shift of the band at 1572 cm^{-1} could be due to the stronger band characteristic of SP originally at 1585 cm^{-1} (N–H bending of primary and secondary amines).[42,51,55,56] Clearly, the inclusion of MMT or SPT disrupted the interaction between chitosan and SP and possibly led to some degree of incompatibility between the two biopolymers.

Figure 4 shows that the mechanical properties of the biopolymers were strongly affected by inclusion of MMT, SPT and SP. All the samples have very small ε_b, indicating their brittle nature. DMTA (see Fig. S1) shows that for CS, CS/M1.5 and CS/SP1.5 the α-transition (glass transition) temperatures were about 45 °C; and for CSSP, CSSP/M1.5 and CSSP/S1.5 the α-transition occurred at even higher temperatures. Thus, the DMTA results indicate the glassy state of samples at RT, corresponding to their brittleness. Compared with CS (E = 1454 ± 243, σ_t = 46.1 ± 6.9 MPa, ε_b = 12.5% ± 4.2%), CS/M1.5 displayed significantly higher σ_t (66.7 ± 5.1 MPa) but similar E and ε_b. CS/M3.0 also had higher σ_t (54.5 ± 6.1 MPa) but lower E (1089 ± 438 MPa). This indicates that the reinforcement of the biopolymers was greater when the MMT loading was 1.5 wt% than at 3.0 wt%. CS/S1.5 had E = 1061 ± 197, σ_t = 53.9 ± 2.0 MPa and ε_b = 14.8% ± 3.1%, and for CS/S3.0, E = 1268 ± 359, σ_t = 50.3 ± 3.5 MPa and ε_b = 7.0% ± 0.1%. This suggests that SPT had no greater effect than MMT in reinforcing the chitosan matrix. A higher SPT content (3 wt%) made the material even more brittle. Thus, the two-dimensional layered structure of MMT and larger surface area were more effective than the one-dimensional SPT nanoneedles in enhancing the mechanical properties of the chitosan matrix.

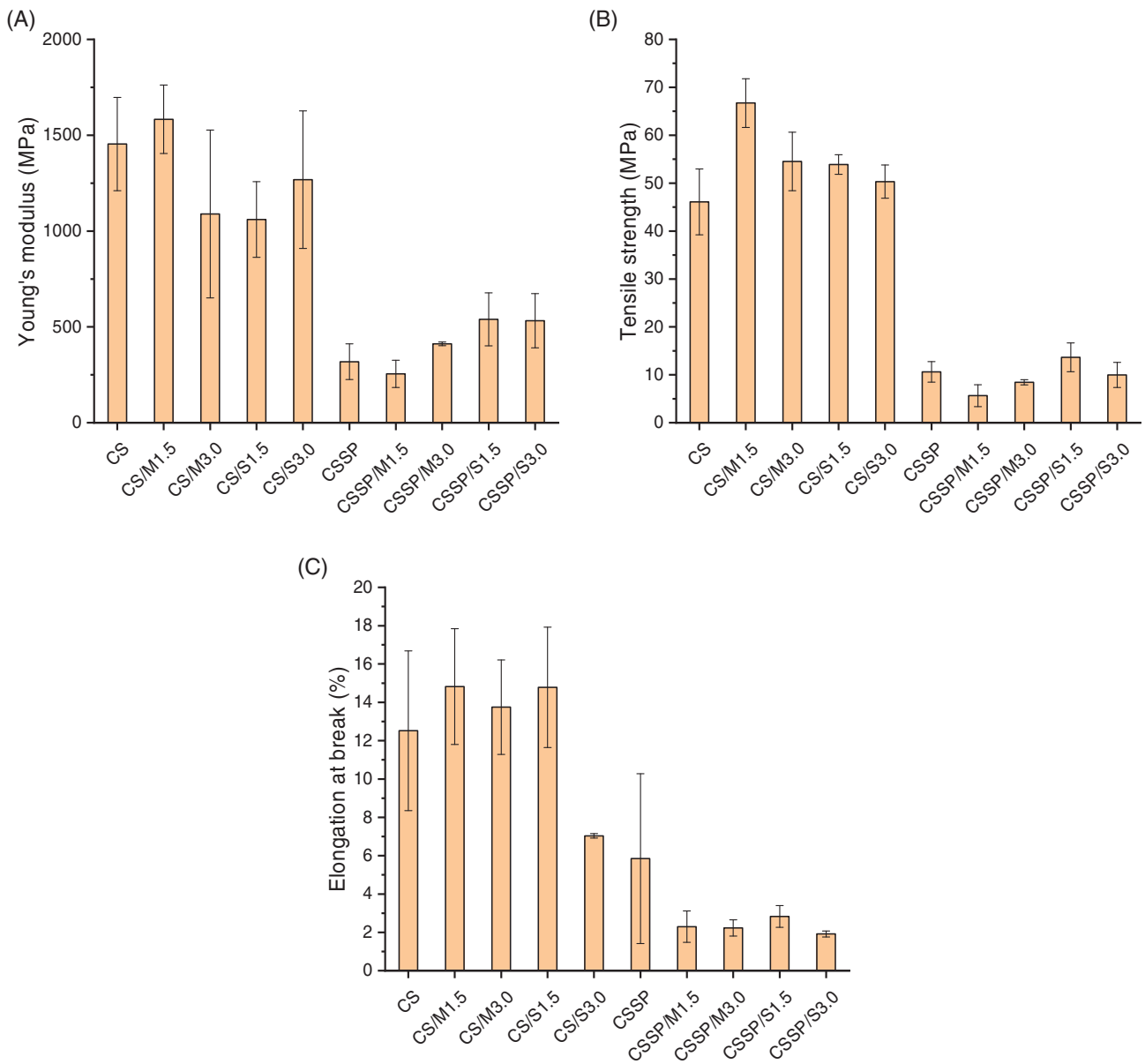

Figure 4. Mechanical properties ((a) Young's modulus E; (b) tensile strength σ_t; (c) elongation at break ε_b) of the chitosan and chitosan/SP films with different MMT/SPT content (0 wt%, 1.5 wt% and 3.0 wt%). The error bars represent standard deviations.

Polymer International published by John Wiley & Sons Ltd on behalf of Society of Industrial Chemistry.

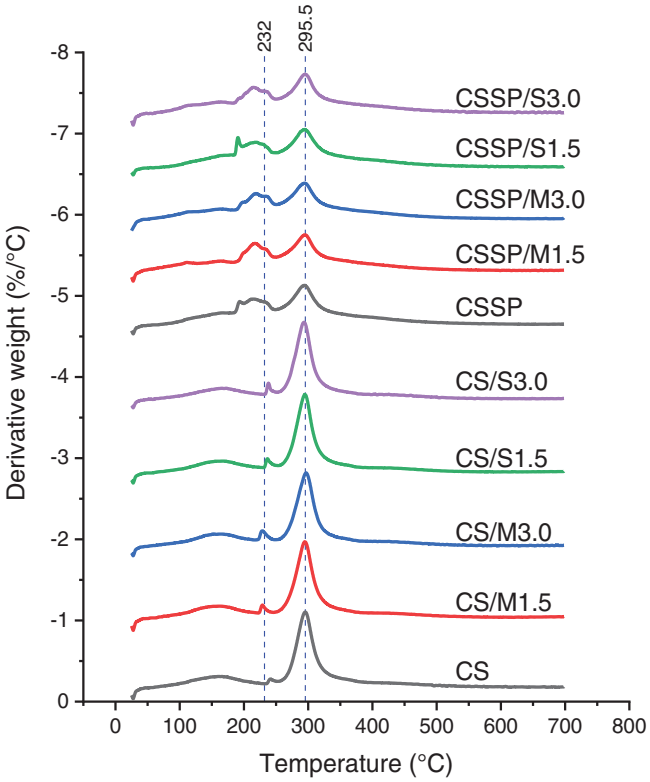

Figure 5. Derivative-weight curves for the chitosan and chitosan/SP films with different MMT/SPT content (0 wt%, 1.5 wt% and 3.0 wt%). The reference lines indicate the maximum thermal decomposition temperatures of SP and chitosan, respectively.[38]

Compared with CS, CSSP exhibited much lower E (319 ± 93 MPa), σ_t (10.6 ± 2.1 MPa) and ε_b (5.9% ± 4.4%), indicating its poorer mechanical properties, behaviour that could be attributed to the low-molecular-mass SP. Inclusion of MMT in the chitosan/SP matrix did not bring an improvement in mechanical properties. In the blend matrix, the MMT nanosheets were not adequately delaminated (see the XRD results) such that no reinforcement was achieved. However, modest improvements in mechanical properties were achieved by the inclusion of SPT. Specifically, CSSP/S1.5 displayed higher E (540 ± 138 MPa) and σ_t (13.7 ± 3.0 MPa) and CSSP/S3.0 also had higher E (532 ± 141 MPa). In this regard, SPT as a needle-like clay was more effective than the MMT platelets at enhancing the mechanical properties of the chitosan/SP matrix, which could be due to it being better dispersed.

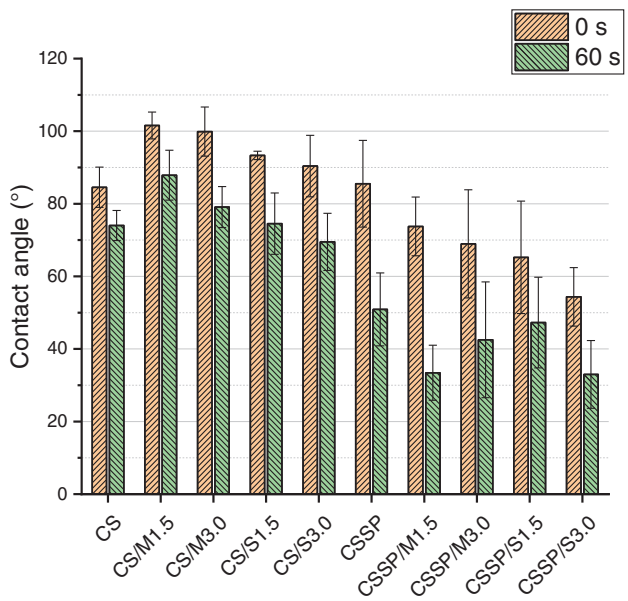

Figure 6. Contact angle values for the chitosan and chitosan/SP films with different MMT/SPT content (0 wt%, 1.5 wt% and 3.0 wt%). The error bars represent standard deviations.

Regarding thermal stability, our previous study[38] indicated that unprocessed chitosan had a major decomposition peak spanning from about 200 °C to 400 °C on the derivative-weight curve, with a peak temperature at 296 °C. SP also displayed a broad thermal decomposition peak from about 130 °C to 470 °C, with a doublet at 221 °C and 232 °C. Figure 5 shows that all the chitosan films had a thermal decomposition profile resembling that of unprocessed chitosan.[38] Nonetheless, a small peak was obtained between *ca* 230 °C and 250 °C. This small peak usually appears for processed unplasticised polysaccharides[58–60] and could be due to the initial de-polymerisation of the polysaccharide. The samples that included either MMT or SPT displayed no changes in thermal stability except for CS/M3.0, which showed a very slight increase in the maximum temperature for the major peak.

All the chitosan/SP-based samples exhibited very similar derivative-weight profiles having two major weight-loss processes. The major peak for chitosan (*ca* 295 °C) was readily visible without any change in the peak temperature. At lower temperatures, a decomposition process occurred between 183 °C and 248 °C, which could be ascribed to the main thermal decomposition of SP.[38] Similarly, Kweon *et al.*[47] reported two temperature maxima for the thermal decomposition of chitosan/SF blends. This could be indirect evidence of the incompatibility between chitosan and SF. It can be seen that the SP in the solution-cast films had slightly reduced thermal stability, whereas the effect of the inclusion of MMT/SPT was not evident.

The θ_{c0s} and θ_{c60s} values of the different samples are shown in Fig. 6. CS had θ_{c0s} = 85° ± 6° and θ_{c60s} = 74° ± 4°. In comparison, inclusion of MMT led to reduced surface wettability, with θ_{c0s} = 102° ± 4° and θ_{c60s} = 88° ± 7° for CS/M1.5 and θ_{c0s} = 100° ± 7° and θ_{c60s} = 79° ± 6° for CS/M3.0. While chitosan contains large amounts of polar groups (i.e. –OH and –NH_2) contributing to its high surface hydrophilicity, MMT should be less hydrophilic than chitosan and its layered structure could make chitosan polar groups less exposed on the film surface.[61,62] MMT was more effective at reducing the surface hydrophilicity at 1.5 wt% loading than at 3.0 wt%, which could be ascribed to more MMT agglomerations at the higher content. Compared with CS, CS/S1.5 and CS/S3.0 also had higher θ_{c0s} (93° ± 1° and 90° ± 8°, respectively) but similar θ_{c60s}. In this regard, inclusion of SPT into the chitosan matrix also enhanced the surface hydrophobicity but not as effectively as MMT. The needle-like structure of SPT may not be as effective as the layered structure of MMT at increasing the surface hydrophobicity.

Compared with CS, CSSP has similar θ_{c0s} (86° ± 12°) but much lower θ_{c60s} (51° ± 10°). Thus, inclusion of SP in the matrix greatly increased the surface wettability, behaviour linked to the higher hydrophilicity of SP due to its water solubility and lack of the β-sheet structure (see FTIR and XRD discussions). Inclusion of MMT further increased the surface wettability of the chitosan/SP matrix, with θ_{c0s} = 74° ± 8° and θ_{c60s} = 33° ± 8° for CSSP/M1.5

Polymer International published by John Wiley & Sons Ltd on behalf of Society of Industrial Chemistry.

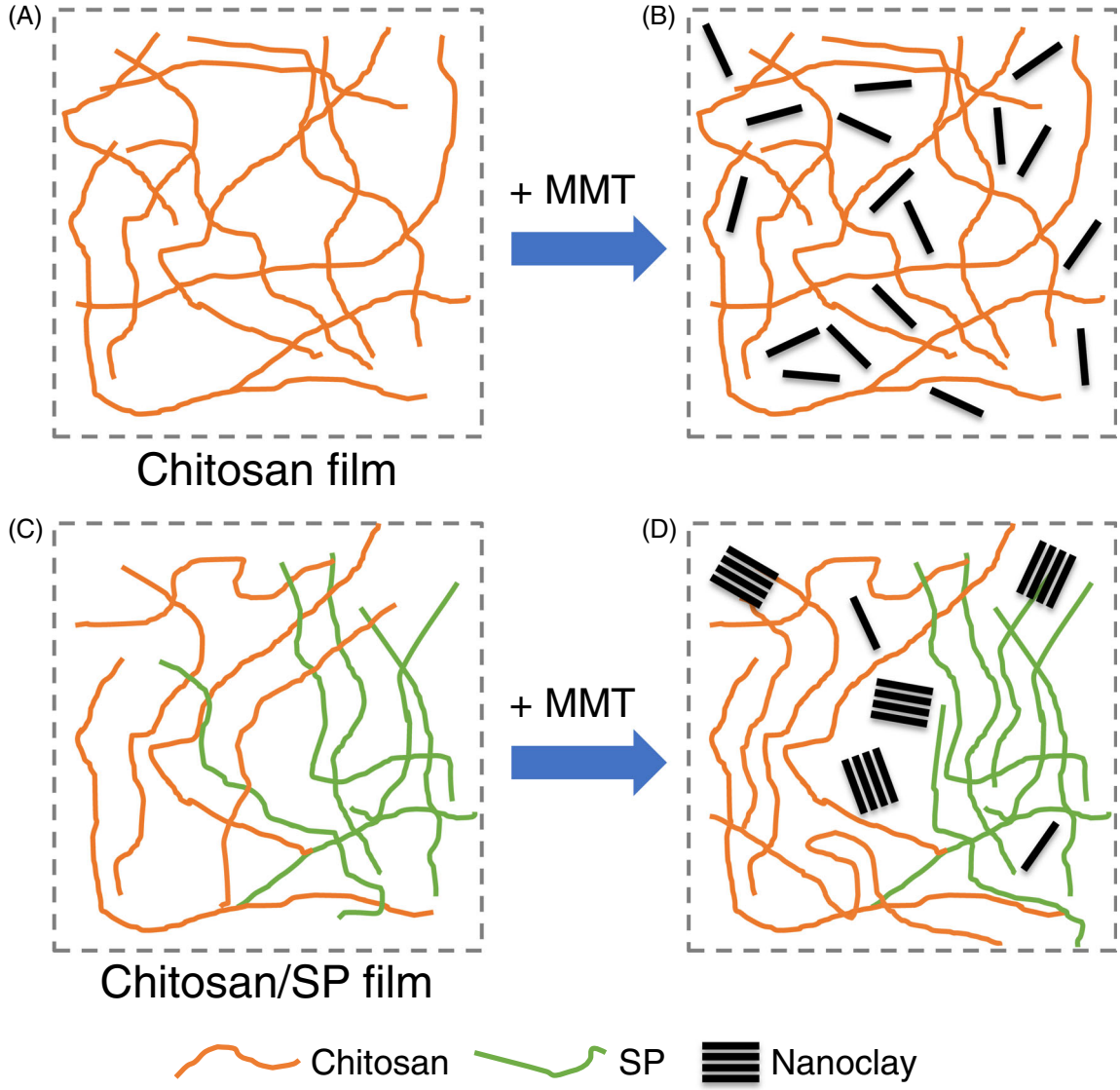

Figure 7. Schematic representation of the structures of solution-cast biopolymer films: (A) chitosan without MMT; (B) chitosan with MMT; (C) chitosan/SP without MMT; (D) chitosan/SP with MMT.

and $\theta_{c0s} = 69° \pm 15°$ and $\theta_{c60s} = 43° \pm 16°$ for CSSP/M3.0. Although the XRD data show that MMT in the hybrid biopolymer matrix was not effectively delaminated, MMT (especially at the 1.5 wt% loading) may still disrupt the inter- and intra-interfacial interactions between the biopolymers, leading to a greater concentration of free biopolymer polar groups. For the chitosan/SP matrix, inclusion of SPT also increased the surface hydrophilicity, with $\theta_{c0s} = 65° \pm 15°$ and $\theta_{c60s} = 47° \pm 12°$ for CSSP/S1.5 and $\theta_{c0s} = 54° \pm 8°$ and $\theta_{c60s} = 33° \pm 9°$ for CS/S3.0. In this regard, SPT nanoneedles also disrupted the biopolymer chain interactions, resulting in a greater concentration of polar groups exposed. This effect was even stronger with a higher SPT content (3.0 wt%).

Figure 7 is a schematic representation of our physical interpretation of the structures of solution-cast chitosan and chitosan/SP films with and without MMT.

The incompatibility between chitosan and proteins could be an issue for materials formation. Some studies[63,64] indicated that chitosan and SF were compatible only when the chitosan weight fraction was less than 0.5. In this current work, films based on chitosan and SP were successfully prepared by solution casting, without apparent phase separation on the micron length scale (see SEM images, Fig. 1). However, the interactions between the two biopolymers are weak (see Fig. 7(C)). This could also be seen from the chitosan/SP materials showing a strong crystalline pattern for SP as well as the separate thermal decomposition events for chitosan and SP. Nonetheless, in our previous work[38] where chitosan/SP materials were prepared by thermomechanical processing and the blended mixture was highly viscous, the crystalline pattern of SP in the blend was not observed. Thus, it is likely that, in a low viscosity solution environment, chitosan and SP chains (which are not fully compatible due to their differences in chemical structure and hydrophilicity/hydrophobicity) tended to undergo chain assembly separately.

The SEM images show that the nanoclay agglomerates were more evident in the chitosan/SP matrix than in the chitosan matrix. In the chitosan matrix, positively charged chitosan could adequately interact with the negatively charged nanoclays,[33,37]

Polymer International published by John Wiley & Sons Ltd on behalf of Society of Industrial Chemistry.

thus acting as a surfactant to assist delamination of the MMT nanosheets (see Fig. 7(B)). Dang *et al.*[39] suggested that SP, when the pH is below its pI, is positively charged and can interact with MMT strongly, facilitating dispersion. However, in this current study, both nanoclays were less finely dispersed in the chitosan/SP matrix as shown by the SEM images and XRD data. In this regard, the two biopolymers may probably interfere with how each interacts with the nanoclay by, for example, forming some kind of aggregated structure. Meanwhile, in the chitosan/SP/nanoclay system, the nanoclay can weaken the interactions between chitosan and SP (see Fig. 7(D)) resulting in some degree of incompatibility between the two biopolymers. This can be seen from the strong FTIR absorption bands of SP in the chitosan/SP-based samples containing a nanoclay. Also, addition of either MMT or SPT to the chitosan/SP matrix interrupted the hydrogen bonding between the biopolymers, increasing the concentration of free polar groups, as reflected by increased surface wettability.

CONCLUSIONS

This work reveals the different effects that nanoclays (MMT and SPT) have on the structure and properties of solution-cast chitosan and chitosan/SP films. No apparent phase separation between chitosan and SP was observed on a microscopic level. Nonetheless, some degree of heterogeneity or incompatibility existed in such materials, confirmed from XRD, FTIR and TGA results. Inclusion of nanoclay in the chitosan/SP matrix had a limited effect on promoting interactions between the two biopolymers, yielding materials with even greater surface wettability. The nanoclay particles in the chitosan/SP matrix were not dispersed as effectively as in the chitosan matrix alone, suggesting that both biopolymers played a role in delamination of the nanoclay. For the chitosan matrix, MMT was more effective than SPT at enhancing mechanical properties, whereas, for the chitosan/SP matrix, mechanical reinforcement was only obtained for SPT, probably due to it being better dispersed in the matrix. While it is common to have multiphasic biopolymer systems (e.g. chitosan and protein) with combined functionality for specific applications (e.g. biomedical), chitosan/silk peptide/nanoclay materials with tailored mechanical properties and hydrophilicity could have potential in wound healing and tissue engineering.

ACKNOWLEDGEMENTS

The authors acknowledge funding from the European Union's Horizon 2020 research and innovation programme under the Marie Skłodowska-Curie grant agreement no. 798225. P. Chen acknowledges the financial support from the Chinese Scholarship Council (CSC) for her visiting position and thanks WMG, University of Warwick, UK, for hosting her research visit. F. Xie also acknowledges support from the Guangxi Key Laboratory for Polysaccharide Materials and Modification, Guangxi University for Nationalities, China (grant no. GXPSMM18ZD-02).

SUPPORTING INFORMATION

Supporting information may be found in the online version of this article.

REFERENCES

1 Rinaudo M, *Prog Polym Sci* **31**:603–632 (2006).
2 Tharanathan RN and Kittur FS, *Crit Rev Food Sci Nutr* **43**:61–87 (2003).
3 Rabea EI, Badawy MET, Stevens CV, Smagghe G and Steurbaut W, *Biomacromolecules* **4**:1457–1465 (2003).
4 Kong M, Chen XG, Xing K and Park HJ, *Int J Food Microbiol* **144**:51–63 (2010).
5 Badawy MEI and Rabea EI, *Int J Carbohydr Chem* **2011**:460381 (2011).
6 Verlee A, Mincke S and Stevens CV, *Carbohydr Polym* **164**:268–283 (2017).
7 Hsu S-h, Wang M-C and Lin J-J, *Appl Clay Sci* **56**:53–62 (2012).
8 Shu XZ and Zhu KJ, *Int J Pharm* **201**:51–58 (2000).
9 Cota-Arriola O, Onofre Cortez-Rocha M, Burgos-Hernández A, Marina Ezquerra-Brauer J and Plascencia-Jatomea M, *J Sci Food Agric* **93**: 1525–1536 (2013).
10 Justin R and Chen B, *Carbohydr Polym* **103**:70–80 (2014).
11 Xu T, Gao C, Yang Y, Shen X, Huang M, Liu S *et al.*, *Food Hydrocoll* **84**: 84–92 (2018).
12 Xiang Y, Zhang G, Chi Y, Cai D and Wu Z, *Chem Eng J* **328**:320–330 (2017).
13 Wan Ngah WS, Teong LC and Hanafiah MAKM, *Carbohydr Polym* **83**: 1446–1456 (2011).
14 Gerente C, Lee VKC, Cloirec PL and McKay G, *Crit Rev Environ Sci Technol* **37**:41–127 (2007).
15 Guibal E, *Sep Purif Technol* **38**:43–74 (2004).
16 Varma AJ, Deshpande SV and Kennedy JF, *Carbohydr Polym* **55**:77–93 (2004).
17 Koh JJ, Lim GJH, Zhou X, Zhang X, Ding J and He C, *ACS Appl Mater Interfaces* **11**:13787–13795 (2019).
18 Zhang S, Lu F, Tao L, Liu N, Gao C, Feng L *et al.*, *ACS Appl Mater Interfaces* **5**:11971–11976 (2013).
19 Torres-Giner S, Ocio MJ and Lagaron JM, *Carbohydr Polym* **77**:261–266 (2009).
20 Kweon H, Ha HC, Um IC and Park YH, *J Appl Polym Sci* **80**:928–934 (2001).
21 Zeng S, Liu L, Shi Y, Qiu J, Fang W, Rong M *et al.*, *PLoS One* **10**:e0128658 (2015).
22 Bhardwaj N and Kundu SC, *Carbohydr Polym* **85**:325–333 (2011).
23 Lai G-J, Shalumon KT, Chen S-H and Chen J-P, *Carbohydr Polym* **111**: 288–297 (2014).
24 Yang K-K, Wang X-L and Wang Y-Z, *J Ind Eng Chem* **13**:485–500 (2007).
25 Ali A and Ahmed S, *Int J Biol Macromol* **109**:273–286 (2018).
26 Giannakas A, Grigoriadi K, Leontiou A, Barkoula N-M and Ladavos A, *Carbohydr Polym* **108**:103–111 (2014).
27 Lavorgna M, Attianese I, Buonocore GG, Conte A, Del Nobile MA, Tescione F *et al.*, *Carbohydr Polym* **102**:385–392 (2014).
28 Rhim J-W, Hong S-I, Park H-M and Ng PKW, *J Agric Food Chem* **54**: 5814–5822 (2006).
29 Wang SF, Shen L, Tong YJ, Chen L, Phang IY, Lim PQ *et al.*, *Polym Degrad Stab* **90**:123–131 (2005).
30 Depan D, Kumar B and Singh RP, *J Biomed Mater Res B Appl Biomater* **84B**:184–190 (2008).
31 Celis R, Adelino MA, Hermosín MC and Cornejo J, *J Hazard Mater* **209–210**:67–76 (2012).
32 Chivrac F, Pollet E, Schmutz M and Avérous L, *Biomacromolecules* **9**: 896–900 (2008).
33 Darder M, Colilla M and Ruiz-Hitzky E, *Chem Mater* **15**:3774–3780 (2003).
34 Chivrac F, Pollet E, Schmutz M and Avérous L, *Carbohydr Polym* **80**: 145–153 (2010).
35 Sinha Ray S and Okamoto M, *Prog Polym Sci* **28**:1539–1641 (2003).
36 Sinha Ray S and Bousmina M, *Prog Mater Sci* **50**:962–1079 (2005).
37 Darder M, López-Blanco M, Aranda P, Aznar AJ, Bravo J and Ruiz-Hitzky E, *Chem Mater* **18**:1602–1610 (2006).
38 Chen P, Xie F, Tang F and McNally T, *Nanocomposites* (2020). https://doi.org/10.1080/20550324.2020.1820796.
39 Dang Q, Lu S, Yu S, Sun P and Yuan Z, *Biomacromolecules* **11**: 1796–1801 (2010).
40 Kittur FS, Vishu Kumar AB and Tharanathan RN, *Carbohydr Res* **338**: 1283–1290 (2003).
41 Jin H-J and Kaplan DL, *Nature* **424**:1057–1061 (2003).
42 Lu Q, Hu X, Wang X, Kluge JA, Lu S, Cebe P *et al.*, *Acta Biomater* **6**: 1380–1387 (2010).
43 Phillips DM, Drummy LF, Conrady DG, Fox DM, Naik RR, Stone MO *et al.*, *J Am Chem Soc* **126**:14350–14351 (2004).
44 Lawrie G, Keen I, Drew B, Chandler-Temple A, Rintoul L, Fredericks P *et al.*, *Biomacromolecules* **8**:2533–2541 (2007).
45 Pawlak A and Mucha M, *Thermochim Acta* **396**:153–166 (2003).

46 Chen Z, Mo X, He C and Wang H, *Carbohydr Polym* **72**:410–418 (2008).
47 Kweon H, Um IC and Park YH, *Polymer* **42**:6651–6656 (2001).
48 Chen X, Li W, Zhong W, Lu Y and Yu T, *J Appl Polym Sci* **65**:2257–2262 (1997).
49 Sionkowska A and Płanecka A, *J Mol Liq* **186**:157–162 (2013).
50 Sionkowska A and Płanecka A, *J Mol Liq* **178**:5–14 (2013).
51 Tsukada M, Gotoh Y, Nagura M, Minoura N, Kasai N and Freddi G, *J Polym Sci Part B Polym Phys* **32**:961–968 (1994).
52 Canetti M, Seves A, Secundo F and Vecchio G, *Biopolymers* **28**: 1613–1624 (1989).
53 Iizuka E and Yang JT, *Biochemistry* **7**:2218–2228 (1968).
54 Kweon HY, Um IC and Park YH, *Polymer* **41**:7361–7367 (2000).
55 Jin H-J, Park J, Karageorgiou V, Kim U-J, Valluzzi R, Cebe P *et al*., *Adv Funct Mater* **15**:1241–1247 (2005).
56 Um IC, Kweon H, Park YH and Hudson S, *Int J Biol Macromol* **29**:91–97 (2001).
57 Wilson D, Valluzzi R and Kaplan D, *Biophys J* **78**:2690–2701 (2000).
58 Chen P, Xie F, Tang F and McNally T, *Compos Sci Technol* **189**:108031 (2020).
59 Chen P, Xie F, Tang F and McNally T, *Int J Biol Macromol* **158**:420–429 (2020).
60 Liu P, Li Y, Shang X and Xie F, *Carbohydr Polym* **206**:528–538 (2019).
61 Gierszewska M, Jakubowska E and Olewnik-Kruszkowska E, *Polym Test* **77**:105872 (2019).
62 Lewandowska K, *Int J Biol Macromol* **81**:159–164 (2015).
63 Park SJ, Lee KY, Ha WS and Park SY, *J Appl Polym Sci* **74**:2571–2575 (1999).
64 Sionkowska A, Lewandowska K and Płanecka A, *J Mol Liq* **198**:354–357 (2014).

